Elevated atmospheric CO_2 and vegetation structural changes contributed to GPP increase more than climate and forest cover changes in subtropical forests of China

Tao Chen[1, 2, *], Félicien Meunier[2], Marc Peaucelle[3], Guoping Tang[1, *], Ye Yuan[4], Hans Verbeeck[2]

1. Carbon-Water Research Station in Karst Regions of Northern Guangdong, School of Geography and Planning, Sun Yat-Sen University, Guangzhou 510006, China
2. CAVElab – Computational and Applied Vegetation Ecology, Department of Environment, Ghent University, Ghent 9000, Belgium
3. INRAE, Université de Bordeaux, UMR 1391 ISPA, 33140 Villenave-d'Ornon, France
4. State Key Laboratory of Desert and Oasis Ecology, Xinjiang Institute of Ecology and Geography, Chinese Academy of Sciences, Urumqi 830011, China

*Corresponding to: Tao Chen (chent265@mail2.sysu.edu.cn); Guoping Tang (tanggp3@mail.sysu.edu.cn)

Contents of this file

Text S1 (description of the photosynthesis model)

The photosynthesis of sunlit and shaded leaves A (i.e., A_{sun} (unit: $\mu mol\ m^{-2}\ s^{-1}$) and A_{shade} (unit: $\mu mol\ m^{-2}\ s^{-1}$)) can be calculated as follows:

$$A = min(A_c, A_j) - 0.015 \times V_m \quad \text{(S1)}$$

where A_c denotes the Rubisco-limited gross photosynthesis rate ($\mu mol\ m^{-2}\ s^{-1}$) and is computed as Eq. S2; A_j is the RuBP-limited gross photosynthesis rate ($\mu mol\ m^{-2}\ s^{-1}$) and is calculated as Eq. S3.

$$A_c = V_m \frac{C_i - \Gamma}{C_i + K} \quad \text{(S2)}$$

$$A_j = J \frac{C_i - \Gamma}{4.5C_i + 10.5\Gamma} \quad \text{(S3)}$$

where C_i is the intercellular CO_2 (Pa); K is a function of enzyme kinetics (Pa) and is calculated as $K = K_C \times \left(1 + \frac{O_2}{K_O}\right)$; O_2 is oxygen concentrations in the atmosphere (Pa); K_C and K_O are the Michaelis-Menten constants for CO_2 (Pa) and O_2 (Pa), respectively; Γ denotes the CO_2 compensation point without dark respiration (Pa) and is calculated as $\Gamma = 4.04 \times 1.75^{(T_a-25)/10}$; V_{cmax} is the maximum carboxylation rate ($\mu mol\ m^{-2}\ s^{-1}$) and J represents the electron transport rate ($\mu mol\ m^{-2}\ s^{-1}$). The corresponding formulas for V_m and J are as follows:

$$V_m = V_{cmax25} \times 2.4^{\frac{T_a-25}{10}} f(T_a) f(N) \quad \text{(S4)}$$

$$f(T_a) = \left\{1 + exp\left[\frac{-220000+710\times(T_a+273)}{8.314\times(T_a+273)}\right]\right\}^{-1} \quad \text{(S5)}$$

$$J = (29.1 + 1.64V_m) \times PPFD / \left(PPFD + 2.1 \times (29.1 + 1.64V_m)\right) \quad \text{(S6)}$$

where V_{cmax25} is the maximum carboxylation rate at 25°C ($\mu molm^{-2}s^{-1}$); Ta is air temperature (°C); $f(N)$ is the function of nitrogen (N) and is usually set to 0.5 in BEPS model (Liu et al., 1999; Zhang et al., 2018), which can adjust the photosynthesis rate for foliage nitrogen (Bonan, 1995). The $PPFD$ is the photosynthesis photon flux density ($\mu mol\ m^{-2}\ s^{-1}$).

Table S1 Information description of flux tower sites in subtropical forest ecosystems in China.

Site name	Vegetation type	Longitude	Latitude	Time range	Reference
Ailaoshan (ALS)	Subtropical evergreen broad-leaved forest (EBF)	101.029°E	24.538°N	2009–2013	Qi et al. (2020); Yu et al. (2006)
Dinghushan (DHS)	Subtropical evergreen broad-leaved forest (EBF)	112.534°E	23.174°N	2003–2010	Yu et al. (2006)
Qianyanzhou (QYZ)	Subtropical evergreen needle-leaved forest (ENF)	115.067°E	26.733°N	2003–2010	Yu et al. (2006)

Table S2 The mean ($\pm$ standard deviation) of V_{cmax25} for different plant functional types (PFTs) calculated from the remote sensing-derived V_{cmax25} products (i.e., multi-year average) in China's subtropical forest ecosystems.

PFTs	Unit	EBF	DBF	ENF	MXF
V_{cmax25}	$\mu molm^{-2}s^{-1}$	38.55 ± 10.14	35.70 ± 6.22	38.47 ± 8.32	33.36 ± 7.96

Table S3 Details of the published GPP products were used for model comparison.

Dataset	Time Range	Spatial Resolution	Method	Source	References
MODIS GPP	2000-2022	500 m	The MOD17 Algorithm	https://ladsweb.modaps.eosdis.nasa.gov/archive/allData/6/MOD17A2H/	Running et al. (2015)
EC-LUE GPP	1982–2018	0.05°	Light use efficiency (LUE)-based model	https://doi.org/10.6084/m9.figshare.8942336.v3.	Zheng et al. (2020)
NIRv GPP	1982–2018	0.05°	Machine learning method	https://doi.org/10.6084/m9.figshare.12981977.v2.	Wang et al. (2021)
VPM GPP	2000-2016	0.05°	Light use efficiency (LUE)-based model	https://figshare.com/articles/dataset/Annual_GPP_at_0_5_degree/5048005	Zhang et al. (2017)
BEPS GPP	1982–2019	0.072727°	Process-based biophysical model (original BEPS model)	http://www.nesdc.org.cn/sdo/detail?id=612f42ee7e28172cbed3d809	Chen et al. (2019); He et al. (2021)

Table S4 Comparison of simulated daily GPP vs. observed daily GPP_{EC} for all three sites in each year.

Sites	Time period	R^2	RMSE (g C m^{-2} day^{-1})	MBE (g C m^{-2} day^{-1})
ALS	2009	**0.50**	1.69	-0.01
	2010	0.72	1.56	-0.10
	2011	0.66	1.49	-0.11
	2012	0.53	1.50	-0.14
	2013	0.53	1.57	0.17
	Overall	0.58	1.57	-0.04
DHS	2003	0.44	1.09	0.38
	2004	0.58	0.95	-0.01
	2005	0.65	1.24	0.88
	2006	0.49	1.21	0.44
	2007	0.47	1.16	0.01
	2008	0.43	1.20	-0.22
	2009	0.43	1.21	0.48
	2010	0.49	1.05	0.01
	Overall	0.44	1.17	0.24
QYZ	2003	0.77	1.27	-0.40
	2004	0.85	1.12	0.18
	2005	0.84	1.06	0.03
	2006	0.78	1.42	-0.00
	2007	0.71	1.46	-0.62
	2008	0.79	1.34	-0.38
	2009	0.76	1.40	-0.40
	2010	0.70	1.60	-0.64
	Overall	0.77	1.36	-0.29

Table S5 Comparison of simulated daily NEP vs. observed daily NEP for all three sites in each year.

Sites	Time period	R^2	RMSE (g C m^{-2} day^{-1})	MBE (g C m^{-2} day^{-1})
ALS	2009	0.21	1.69	0.01
	2010	0.20	1.54	0.04
	2011	0.21	1.49	-0.07
	2012	0.37	1.21	-0.10
	2013	0.24	1.29	0.27
	Overall	0.25	1.46	0.02
DHS	2003	0.41	1.08	0.37
	2004	0.45	0.95	-0.01
	2005	0.42	1.25	0.86
	2006	0.38	1.21	0.42
	2007	0.26	1.16	-0.01
	2008	0.26	1.20	-0.18
	2009	0.49	1.21	0.54
	2010	0.38	1.05	0.01
	Overall	0.35	1.14	0.24
QYZ	2003	0.33	1.27	0.04
	2004	0.57	1.12	0.17
	2005	0.54	1.06	0.03
	2006	0.48	1.42	0.07
	2007	0.36	1.46	-0.04
	2008	0.46	1.31	0.12
	2009	0.36	1.40	0.04
	2010	0.27	1.60	-0.09
	Overall	0.42	1.34	0.04

Table S6 Land-cover change transition matrix for the 2001–2018 period in the subtropical region of China. EBF: evergreen needle-leaved forest; DBF: deciduous broad-leaved forest; ENF: evergreen needle-leaved forest; MF: mixed forest; CRO: cropland; GRA: grassland; SHR: shrubland; URB: urban; and BAR: bare land. Green and red arrows indicate a net increase and a net decrease, respectively.

		2018 ($\times10^3$ km^2)										
		EBF	**DBF**	**ENF**	**MXF**	**CRO**	**GRA**	**SHR**	**URB**	**BAR**	**Total**	**Losses**
2001 ($\times10^3$ km^2)	**EBF**	551.08	0.38	1.72	7.79	3.03	0.13	0.42	0.00	0.10	564.66	13.57
	DBF	0.64	89.62	0.16	2.97	0.26	0.03	0.03	0.03	0.00	93.74	4.12
	ENF	3.48	0.06	492.41	19.04	13.10	0.80	0.32	0.29	0.03	529.52	37.11
	MXF	8.50	1.12	10.73	275.61	3.00	0.48	0.13	1.72	0.16	301.44	25.84
	CRO	12.33	2.14	4.18	4.63	1089.49	0.80	0.64	34.75	1.53	1150.49	61.00
	GRA	0.29	0.10	1.57	1.98	0.67	127.85	0.00	4.95	0.10	137.50	9.65
	SHR	5.59	0.67	2.17	1.02	3.39	0.10	9.58	0.22	0.10	22.84	13.25
	URB	0.00	0.00	0.00	0.00	0.03	0.00	0.00	23.76	0.00	23.79	0.03
	BAR	0.10	0.03	0.00	0.06	0.67	0.10	0.83	0.93	56.18	58.90	2.71
	Total	582.00	94.13	512.95	313.10	1113.63	130.28	11.95	66.66	58.19	–	–
	Gains	30.92	4.50	20.54	37.50	24.15	2.43	2.36	42.89	2.01	–	–
	Net changes	**17.34↑**	**0.38↑**	**-16.58↓**	**11.66↑**	**-36.86↓**	**-7.22↓**	**-10.89↓**	**42.86↑**	**-0.70↓**	–	–

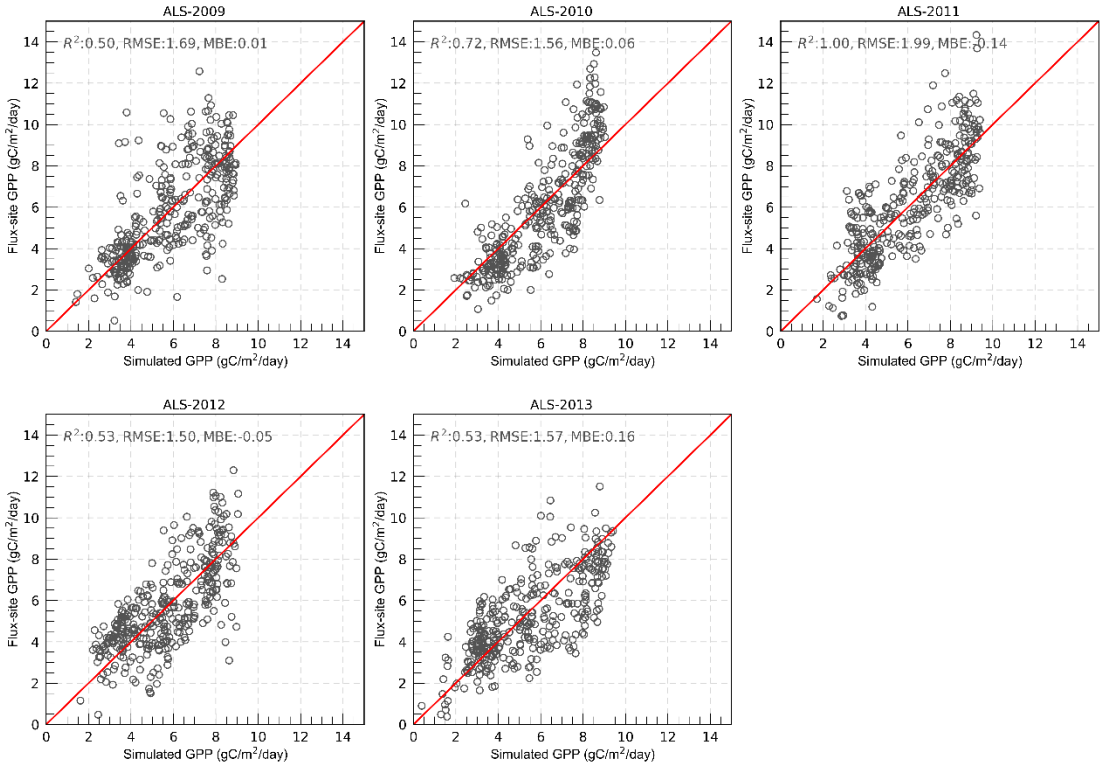

160

Figure S1 Scatter plots show the year-to-year (2009-2013) comparison between the simulated and observed daily GPP in the Ailao Shan flux tower station (ALS). The red line denotes the 1:1 line.

165

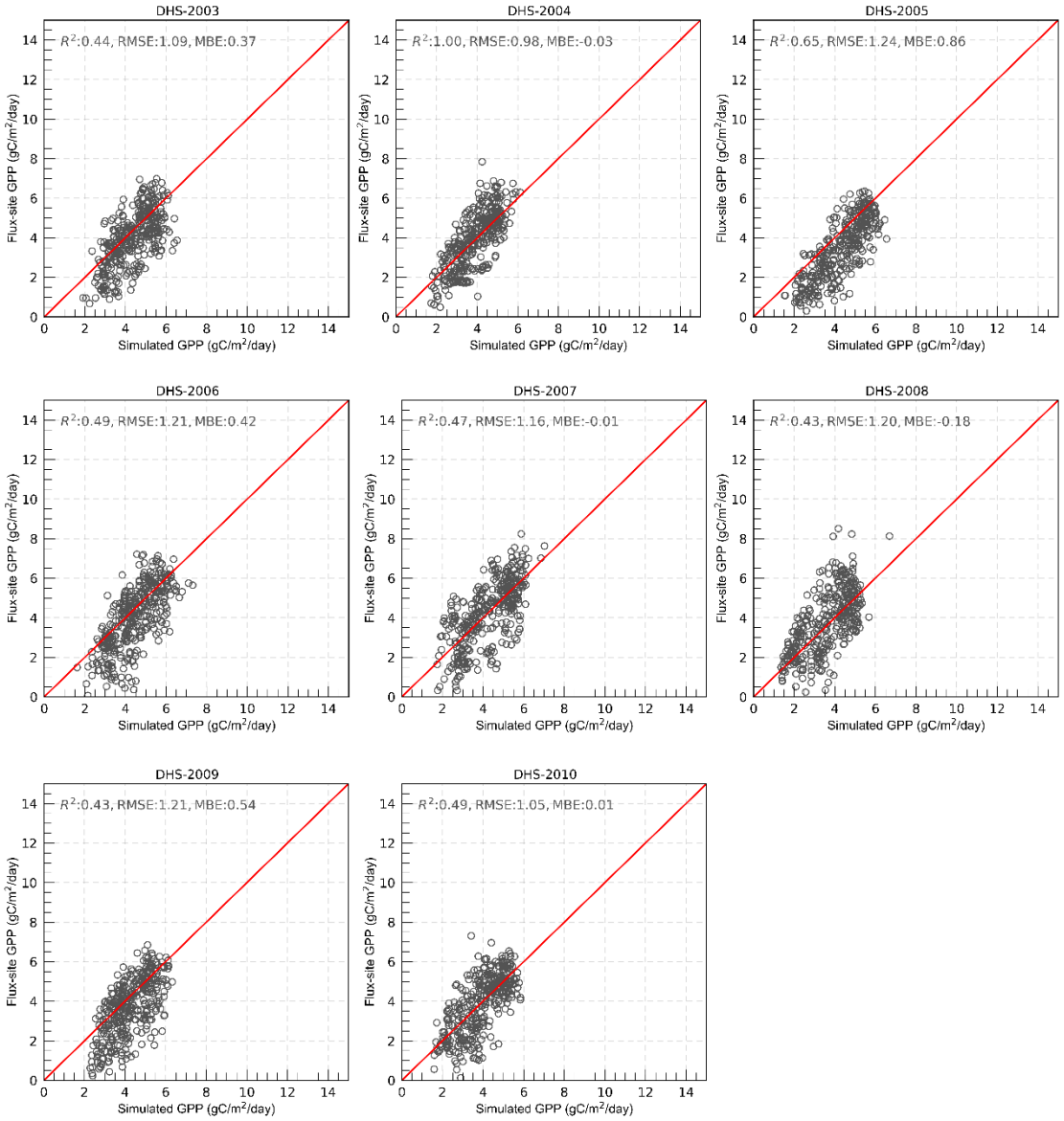

Figure S2 Scatter plots show the year-to-year (2003-2010) comparison between the daily simulated GPP with observed GPP in Dinghu Shan flux tower station (DHS).

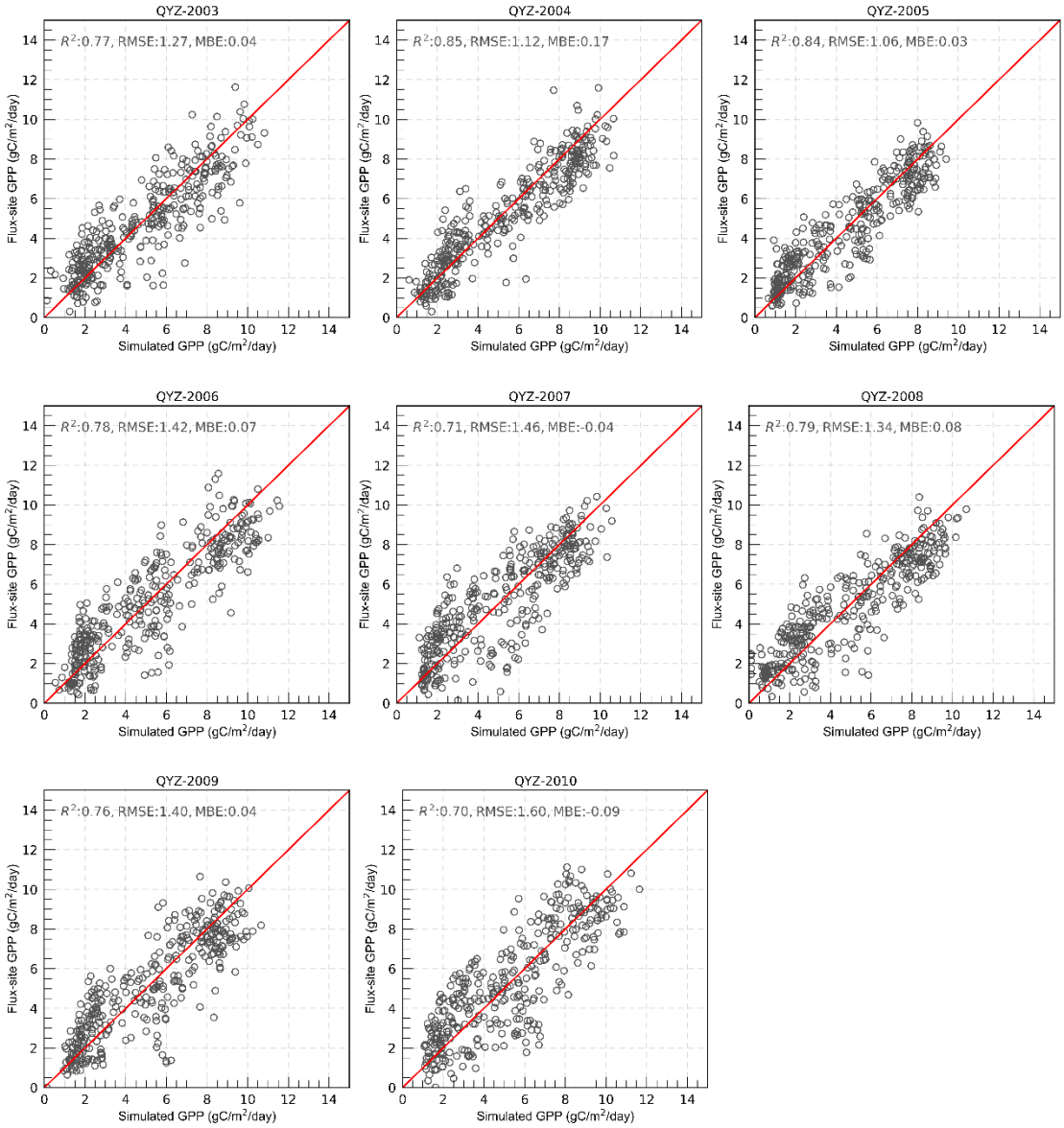

Figure S3 Scatter plots show the year-to-year (2003-2010) comparison between the daily simulated GPP with observed GPP in Qianyan Zhou flux tower station (QYZ).

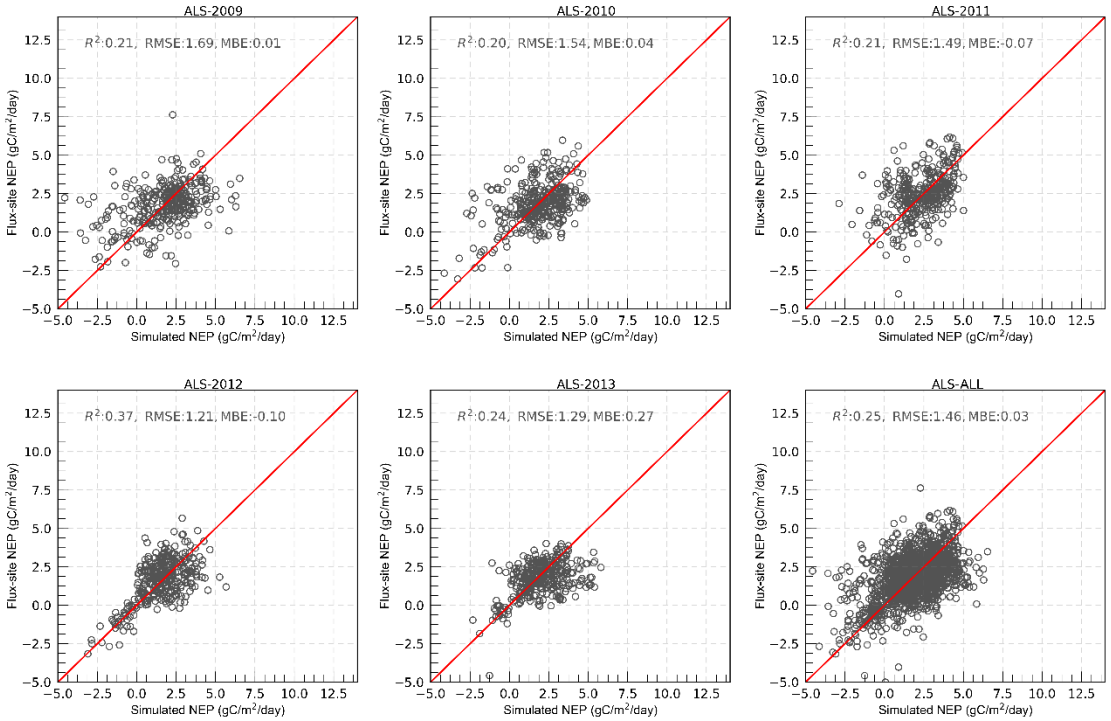

Figure S4 Scatter plots show the year-to-year (2009-2013) comparison between the daily simulated NEP with observed NEP in the Ailao Shan flux tower station (ALS). The red line denotes the 1:1 line.

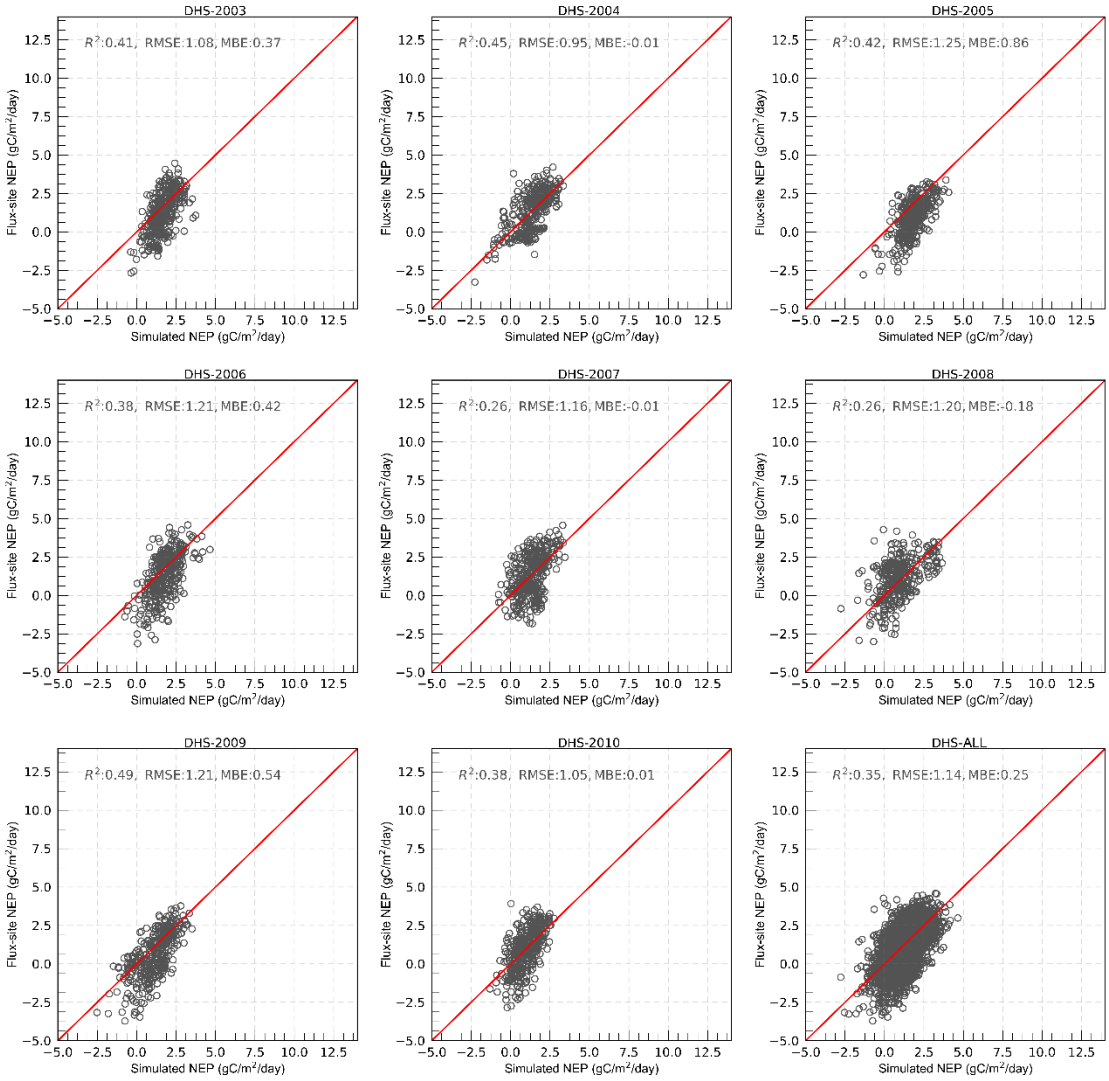

Figure S5 Scatter plots show the year-to-year (2003-2010) comparison between the daily simulated NEP with observed NEP in Dinghu Shan flux tower station (DHS). The red line denotes the 1:1 line.

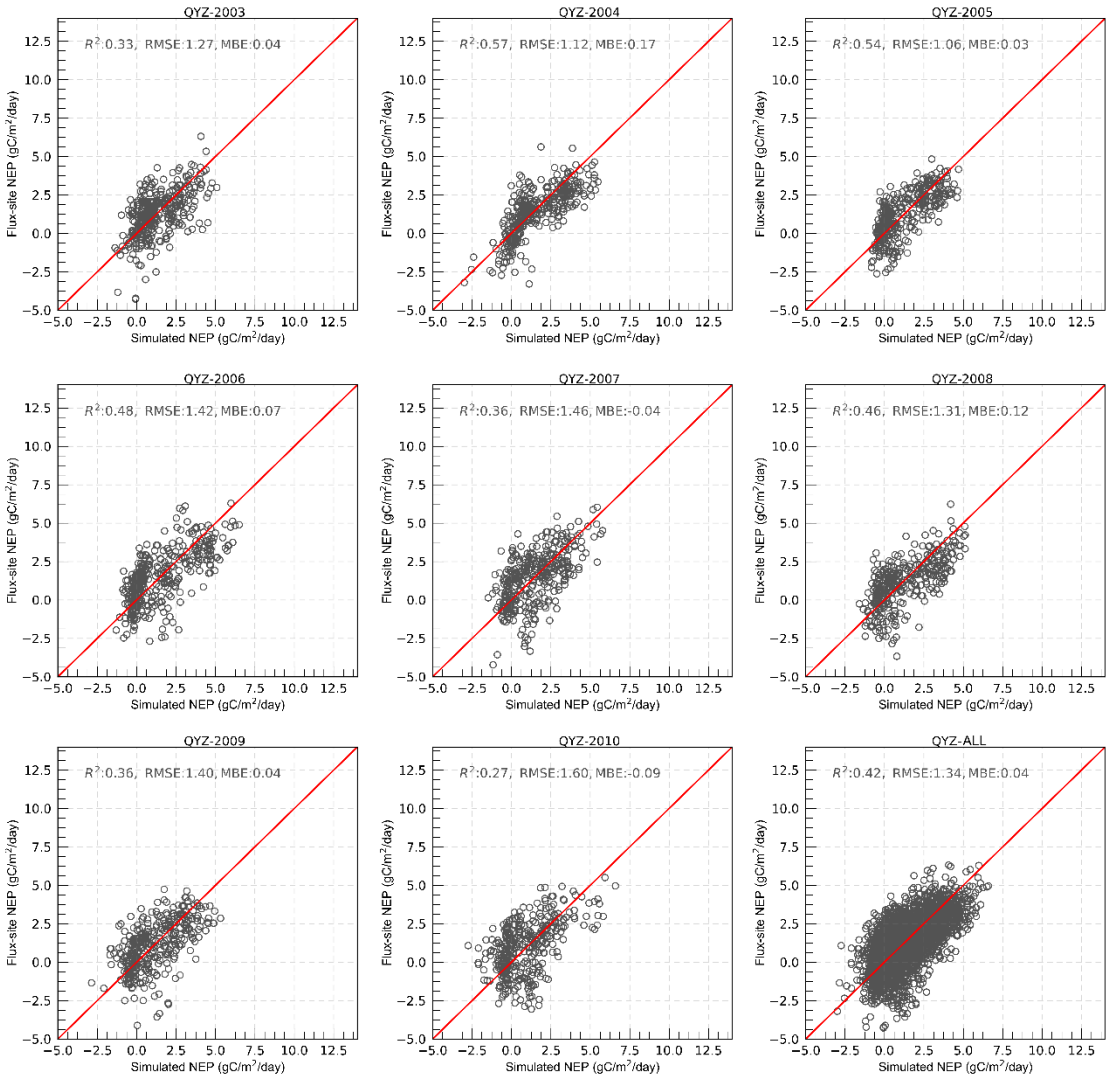

Figure S6 Scatter plots show the year-to-year (2003-2010) comparison between the daily simulated NEP with observed NEP in Qianyan Zhou flux tower station (QYZ). The red line denotes the 1:1 line.

220

225

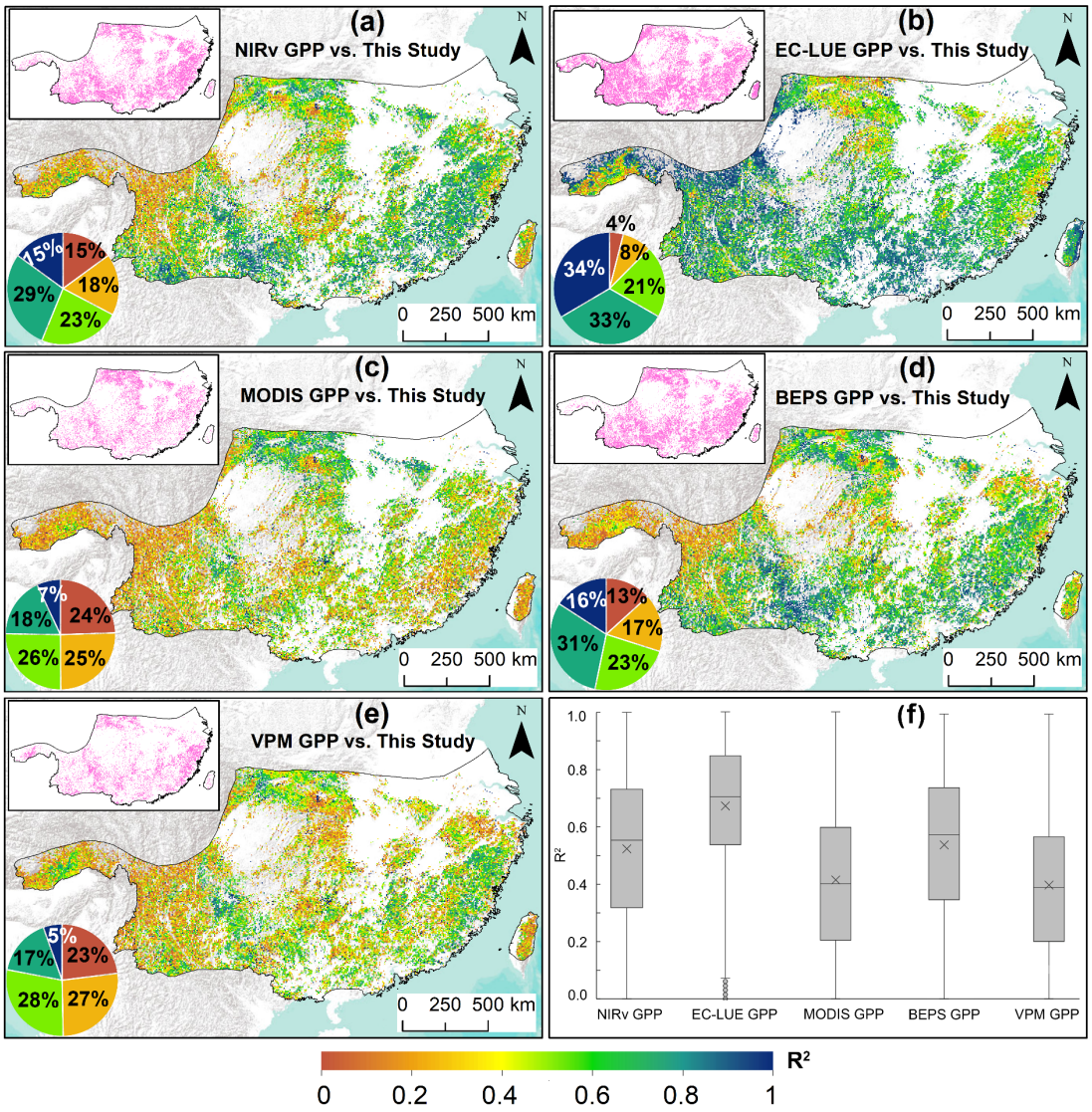

Figure S7 Spatial distribution of the determination coefficient (R^2) between our simulated GPP and five GPP products at annual scale (a-e). The insert pie charts represent the ratios of different R^2, which corresponds to the color bar. (f) Box chart is statistical results of R^2 between our simulated GPP and five GPP products. The black horizontal line in the boxplot is the median, and the cross represents the mean. Insets in (a-e) represent the subset of pixels where our simulated GPP is significantly correlated with the five GPP products at the $P < 0.05$ confidence level.

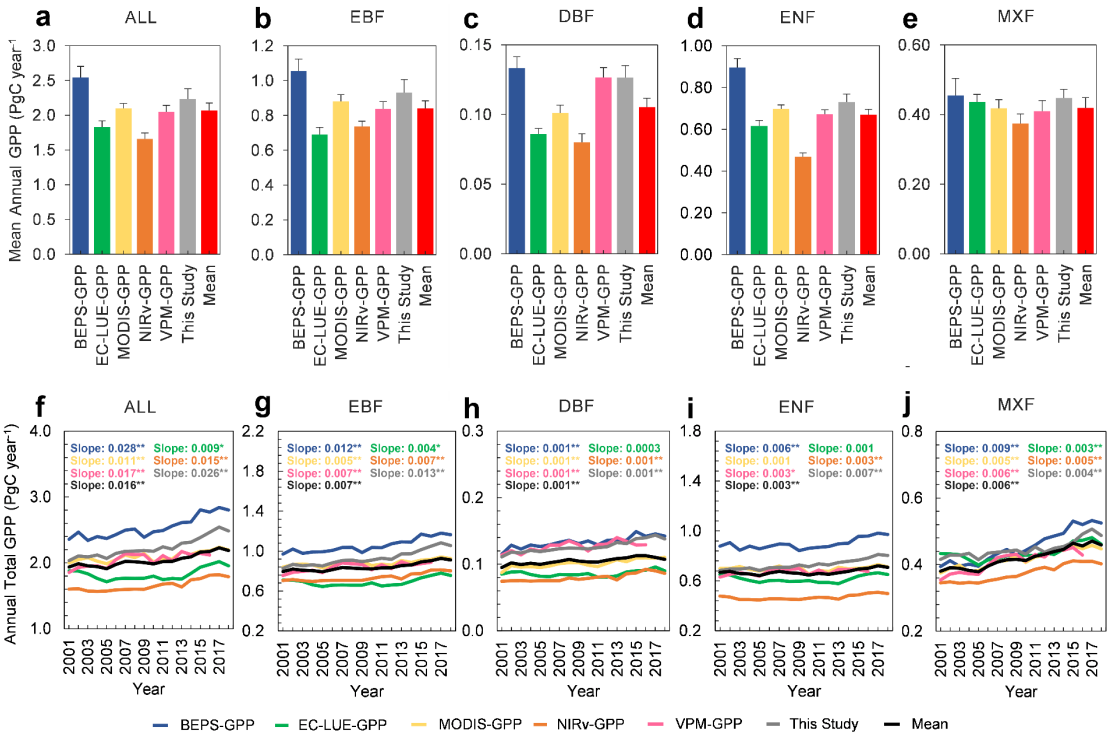

Figure S8 Comparison of the multi-year mean of annual total GPP (a-e) and the annual GPP trends (f-g) between our simulated GPP and other five published GPP products for the entire study area and different forest types. The VPM GPP can be available from 2001 to 2016 and thus the multi-year mean of annual VPM is calculated from the period 2001-2016. The grey bar in (a-e) is the standard deviation (SD). The mean denotes the average of five products. EBF: evergreen needleleaf forest; DBF: deciduous broadleaf forest; ENF: evergreen needleleaf forest; MF: mixed forest.

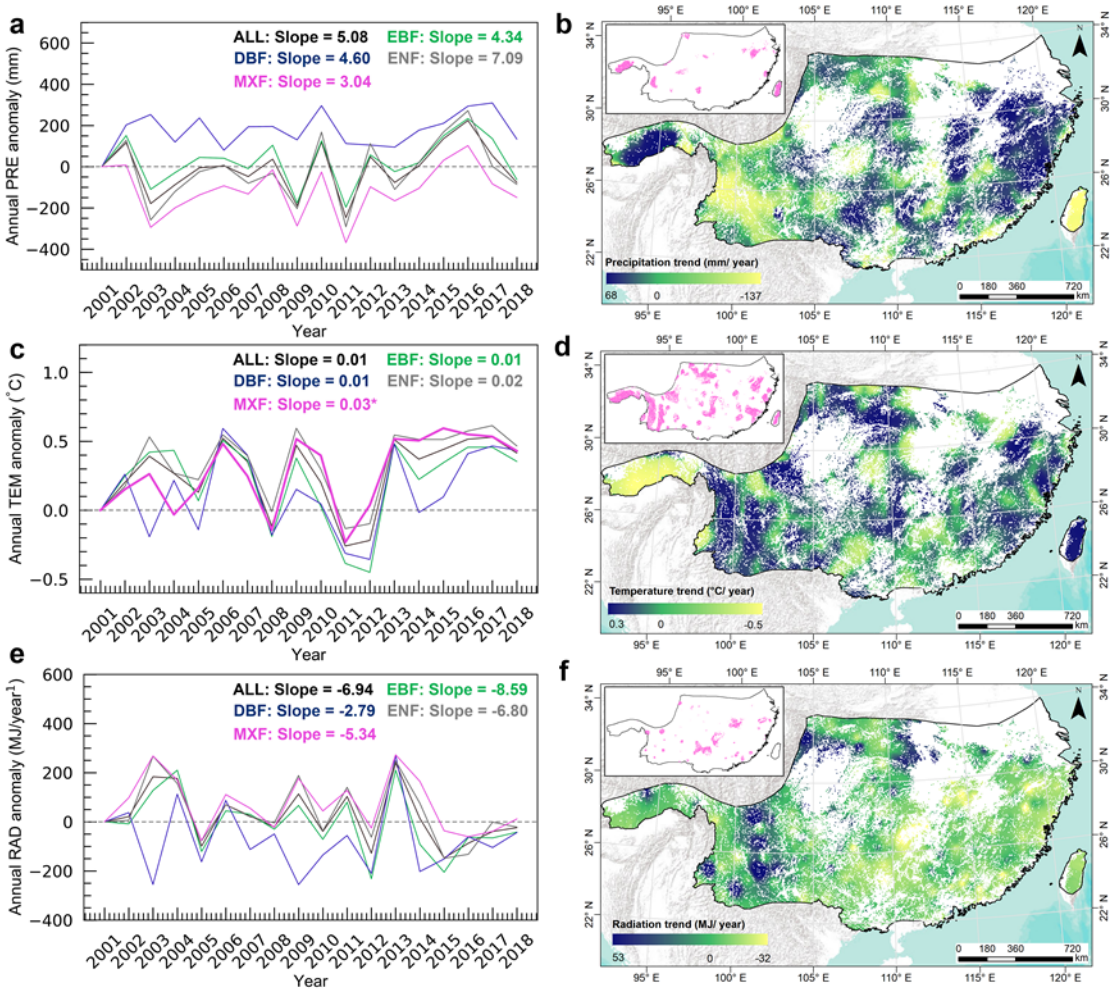

Figure S9 Annual variations of the major climate variables on the entire forest area and different forest areas from 2001 to 2018. The left column is the temporal changes of annual total precipitation anomaly (a), annual mean temperature anomaly (c), and annual total radiation anomaly (e), respectively. The right column is the spatial distribution of annual total precipitation trends (b), annual mean temperature trends (d), and annual total radiation trends (f), respectively. The anomalies are all relative to the base year 2001. Insets in (b), (d), and (f) denote the subset of pixels with significant annual precipitation, temperature, and radiation changes at $P < 0.05$. EBF: evergreen needleleaf forest; DBF: deciduous broadleaf forest; ENF: evergreen needleleaf forest; MF: mixed forest.

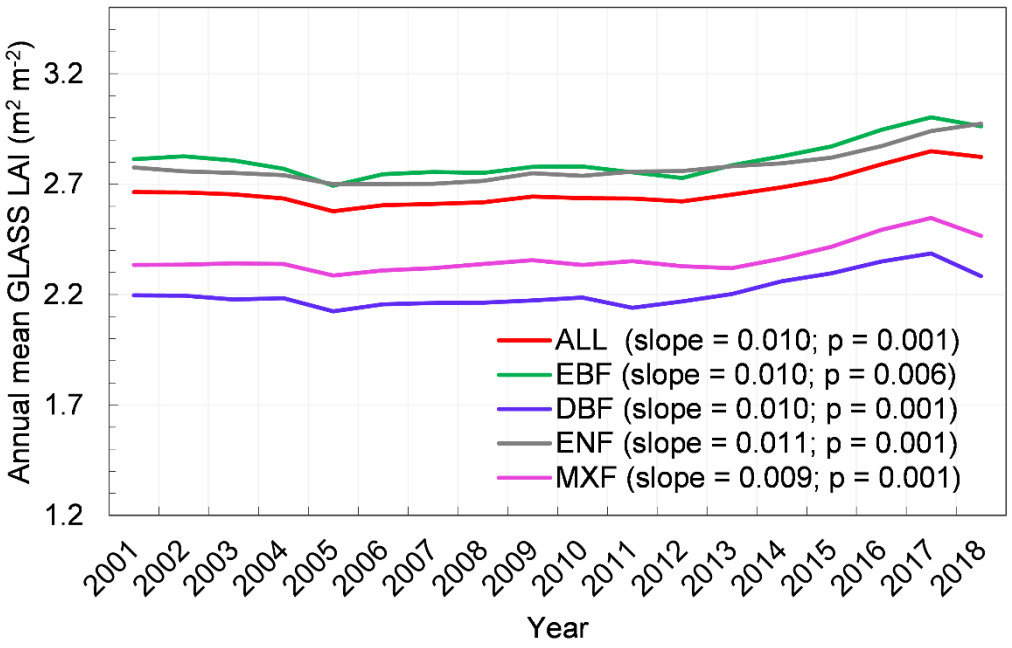

Figure S10 Annual changes of GLASS LAI for entire forest region and different forest types. EBF: evergreen needleleaf forest; DBF: deciduous broadleaf forest; ENF: evergreen needleleaf forest; MF: mixed forest.

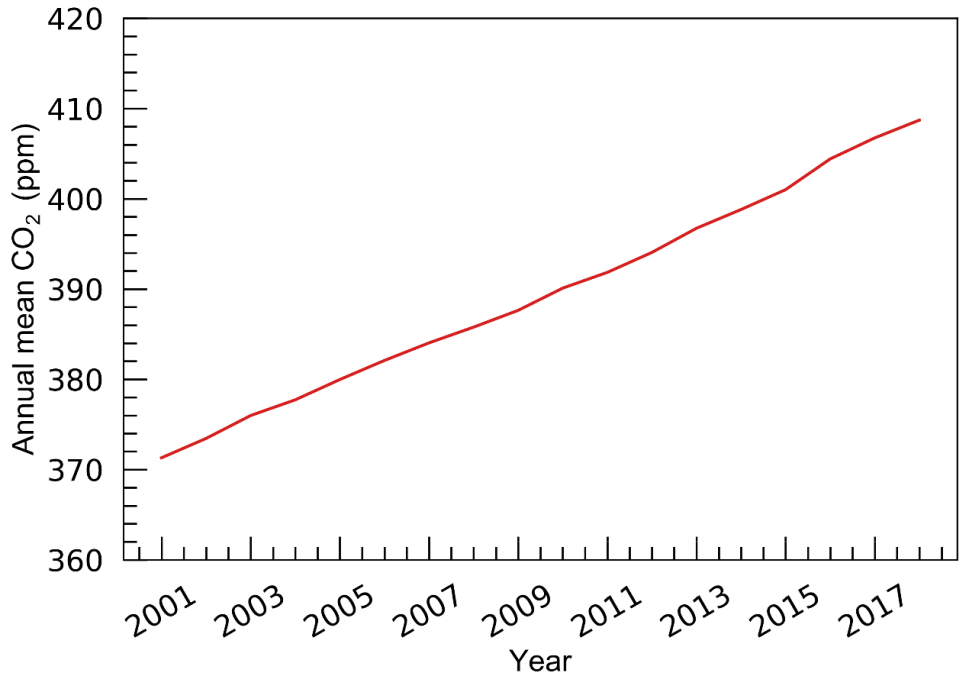

Figure S11 Temporal changes of annual mean CO_2 concentration from 2001 to 2018.

References

Bonan, G.B., 1995. Land-atmosphere CO2 exchange simulated by a land surface process model coupled to an atmospheric general circulation model Journal of Geophysical Research, 100(D2): 2817-2831.

Chen, J.M., Ju, W., Ciais, P., Viovy, N. and Lu, X., 2019. Vegetation structural change since 1981 significantly enhanced the terrestrial carbon sink. Nature Communications, 10(1): 4259.

He, Q. et al., 2021. Drought Risk of Global Terrestrial Gross Primary Productivity Over the Last 40 Years Detected by a Remote Sensing-Driven Process Model. Journal of Geophysical Research: Biogeosciences, 126(6): e2020JG005944.

Liu, J., Chen, J.M., Cihlar, J. and Chen, W., 1999. Net primary productivity distribution in the BOREAS region from a process model using satellite and surface data. Journal of Geophysical Research: Atmospheres, 104(D22): 27735-27754.

Qi, D. et al., 2020. A dataset of carbon and water fluxes observation in subtropical evergreen broad-leaved forest in Ailao Shan from 2009 to 2013. China Scientific Data, 6(1). (2021-03-06). DOI: 10.11922/csdata.2020.0089.zh.

Running, S.W., Mu, Q. and Zhao, M., 2015. MOD17A2H MODIS/Terra Gross Primary Productivity 8-Day L4 Global 500m SIN Grid. NASA LP DAAC. http://doi.org/10.5067/MODIS/MOD17A2H.006.

Wang, S., Zhang, Y., Ju, W., Qiu, B. and Zhang, Z., 2021. Tracking the seasonal and inter-annual variations of global gross primary production during last four decades using satellite near-infrared reflectance data. Sci Total Environ, 755(Pt 2): 142569.

Yu, G.-R. et al., 2006. Overview of ChinaFLUX and evaluation of its eddy covariance measurement. Agricultural and Forest Meteorology, 137(3-4): 125-137.

Zhang, Y. et al., 2017. A global moderate resolution dataset of gross primary production of vegetation for 2000-2016. Scientific Data, 4: 170165.

Zheng, Y. et al., 2020. Improved estimate of global gross primary production for reproducing its long-term variation, 1982–2017. Earth System Science Data, 12(4): 2725-2746.

Zhang, S. et al., 2018. Evaluation and improvement of the daily boreal ecosystem productivity simulator in simulating gross primary productivity at 41 flux sites across Europe. Ecological Modelling, 368: 205-232.